

Interpreting the HI 21-cm cosmology maps through Largest Cluster Statistics – III: Impact of the lightcone effect

Hemanth Potluri,^{a,b,c} Manas Mohit Dosibhatla,^a Leon Noble,^a Chandra Shekhar Murmu,^{a,d} Suman Majumdar,^a Samit Kumar Pal,^a Saswata Dasgupta,^e Satadru Bag,^{f,g} Abhirup Datta^a

^aDepartment of Astronomy, Astrophysics and Space Engineering, Indian Institute of Technology Indore, Khandwa Road, Indore - 453552, India

^bDepartment of Physics, Stellenbosch University, Matieland 7602, South Africa

^cKapteyn Astronomical Institute, University of Groningen, PO Box 800, NL-9700 AV Groningen, the Netherlands

^dAstrophysics Research Center of the Open University (ARCO) & Department of Natural Sciences, The Open University of Israel, 1 University Road, Ra'anana 4353701, Israel

^eInstitute of Astronomy & Kavli Institute for Cosmology, University of Cambridge, Madingley Road, Cambridge CB3 0HA, United Kingdom

^fPhysics Department, TUM School of Natural Sciences, Technical University of Munich, James-Franck-Straße 1, 85748 Garching, Germany

^gMax-Planck-Institut für Astrophysik, Karl-Schwarzschild Straße 1, 85748 Garching, Germany

E-mail: hemanthpotluri.98@gmail.com, dosibhatla.mohit@gmail.com

Abstract. The redshifted 21-cm signal emitted by neutral Hydrogen (HI) is a promising probe to understand the evolution of the topology of ionized regions during the Epoch of Reionization (EoR). The topology of ionized regions allows us to infer the nature and properties of ionizing sources, i.e., early galaxies and AGNs. Traditional Fourier statistics, such as the power spectrum, help us quantify the strength of fluctuations in this field at different length scales but do not preserve its phase information. Analyzing the 21-cm brightness temperature field in the image domain retains its non-Gaussian characteristics and morphological information. One such approach is to track the coalescence of multiple ionized regions to form one contiguous ionized region spanning the universe. This is referred to as percolation, and its onset is quantified by a sharp rise in the value of the Largest Cluster Statistic (LCS) approaching unity. In this work, we carry out a percolation analysis of 21-cm brightness temperature fields by studying the redshift evolution of the LCS along a lightcone to distinguish between several simulated reionization scenarios. We have extended previous results on reionization model comparison from the analysis of coeval 21-cm maps to understand how the lightcone effect biases the observed percolation behavior and affects the distinguishability of the source models. We estimate the LCS of subvolumes of different sizes in the 21-cm lightcone maps and study their redshift evolution for different reionization scenarios using a moving volume approach. We find that the percolation transition inferred from a lightcone approaches that from the coeval box as we increase the bandwidth of the moving volume in all but one reionization scenario. We conclude that, to distinguish between reionization scenarios through percolation analysis of 21-cm intensity map lightcones observed by SKA-Low, a moving volume with a bandwidth of 15 MHz is optimal.

Keywords: reionization, intergalactic media, cosmological simulations, non-gaussianity

Contents

1	Introduction	1
2	Simulations	3
2.1	Semi-numerical simulation of reionization	3
2.2	Reionization source models and scenarios	4
2.2.1	Reionization source models	4
2.2.2	Reionization Scenarios	5
2.3	Simulating lightcone maps	6
3	Methodology	7
3.1	Percolation analysis	7
3.2	Calculating LCS in lightcone maps	8
4	Results	8
4.1	Percolation analysis on coeval maps	8
4.2	Percolation analysis on fiducial lightcone map	9
4.3	Evolution of LIR in different reionization scenarios	10
5	Summary	12

1 Introduction

The Epoch of Reionization (EoR) refers to the period in the history of the universe when UV and X-ray photons emitted by the first galaxies and active galactic nuclei (AGN) ionized the neutral atomic hydrogen (HI) in the intergalactic medium (IGM) [1–5]. It was the last major phase transition of hydrogen in the universe. Studying the EoR provides key information to understand the evolution of the universe from its early stages with tiny fluctuations in the matter distribution observed through the cosmic microwave background (CMB) radiation [6], to the highly clustered non-Gaussian matter distribution observed in low-redshift galaxy surveys [7, 8]. In addition, the reionization and the associated photo-heating of IGM gas from the ultraviolet background (UVB) affect subsequent galaxy formation [9–11].

Indirect probes, such as observations of quasar spectra [12–14], Thomson scattering optical depth of CMB photons [15], and the luminosity and clustering properties of Lyman alpha (Ly α) emitters [16–19], suggest that reionization is an extended process spanning roughly the redshift range of $6 \lesssim z \lesssim 15$. However, our knowledge about the properties of the sources responsible for the reionization of the universe and the evolution of the topology of ionized regions during this period still remains uncertain. The types of sources responsible for reionization (galaxies and AGNs) and their relative contributions need to be understood in detail to describe reionization completely. The 21-cm line emission from HI atoms resulting from the transition between the triplet and singlet hyperfine states of its ground state is a tracer of the HI distribution in the universe. Constructing tomographic maps of the brightness temperature fluctuations of the 21-cm line using a radio interferometer allows us to identify ionized regions at different redshifts from the cold spots in these maps [2, 20–22]. This

directly tracks the evolution of the topology of ionized regions [23, 24], which are expected to differ across reionization scenarios [25].

Direct detection of the 21-cm intensity mapping signal from the EoR has not been achieved yet because of observational challenges such as astrophysical foregrounds that are 4–5 orders of magnitude larger than the actual signal [26–32], coupled with residual calibration errors [33–36], ionospheric phase errors [37–39], and other instrumental systematics [40]. However, upper limits of the 21-cm power spectrum have been reported through observations using several radio interferometric arrays such as the Giant Metrewave Radio Telescope (GMRT) [41], Precision Array to Probe the Epoch of Reionization (PAPER) [42, 43], Low Frequency ARray (LOFAR) [44–47], Murchison Widefield Array (MWA) [48–50], and Hydrogen Epoch of Reionization Array (HERA) [51]. These upper limits have been used to put constraints on the thermal and ionization history during the EoR and to rule out several exotic reionization models [52–55]. Upper limits have also been reported for higher-order signal statistics such as the bispectrum using the MWA [56]. The low-frequency component of the upcoming Square Kilometre Array (SKA-Low), situated in Western Australia, will have enough sensitivity to construct tomographic maps of the EoR 21-cm signal [57–59].

In order to interpret the observed 21-cm signal from the EoR, the signal statistics need to be modeled and compared with the observed statistics for reionization parameter estimation [60–66] or model selection [67, 68]. Even though the power spectrum, as a summary statistic, quantifies the contribution of different length scales to the signal fluctuations, it can only completely describe Gaussian fields. The EoR 21-cm signal is non-Gaussian [3, 69, 70], and hence higher-order statistics such as the bispectrum need to be estimated for a more adequate description of the signal [71–75].

Fourier domain statistics, however, cannot preserve the full information of the phases of the signal in the Fourier space. This leads to an information loss on the topology of the ionized bubbles in the IGM, and how the ionized regions evolve, grow, and merge to complete the reionization process. This necessitates analyzing the tomographic intensity maps in the image domain to recover more information. Previous efforts at such analysis of 21-cm maps include topology quantifiers such as the Minkowski Functionals [23, 24, 76–79], Shapefinders [80], Minkowski Tensors [81], Betti numbers [82], granulometry [83], persistence theory [84], etc. There have also been multiple efforts to characterize EoR 21-cm maps at the field level [85–93]. An effective way to track the evolution of ionized bubbles is through percolation theory [7, 23–25, 94–98]. This is based on probing the percolation transition of the ionized bubbles, which marks the stage where the small ionized bubbles coalesce to form one large ionized region spanning a simulation box. Extending this with periodic boundary conditions, the largest ionized region (LIR) can be considered to span the entire universe, culminating in large-scale connectivity of ionized regions.

Instead of detecting a large number of ionized regions, detecting the LIR in the simulation box is sufficient to track the percolation process using the Largest Cluster Statistic (LCS) [23]. Previous work by Pathak et al. [25, **Paper I** hereafter] has demonstrated that the multiple reionization source models of [99] with the same global reionization history that can lead to different progression of reionization (inside-out and outside-in [100]) can be distinguished using the LCS. Among previous papers in this series, Dasgupta et al. [96, **Paper IIa** hereafter] studied how the convolution of the target signal with the synthesized beam of SKA-Low affects the inferred percolation transition point. Pal et al. [98, **Paper IIb** hereafter] studied the tolerance level to gain calibration errors in the recovery of the percolation behavior of foreground-contaminated maps.

Papers I, IIa, and IIb utilized coeval simulation boxes for estimating the signal statistics. In reality, the observed signal in different frequency channels originates from different redshifts, i.e., different cosmic times, as a result of the finite time light takes to travel. As a result, the signal evolves across every slice along the line of sight of a tomographic map, introducing biases relative to coeval boxes. This is known as the lightcone effect, and its impact has been studied on the 21-cm power spectrum [101–107] and bispectrum [73]. In this work, we study the bias introduced by the lightcone effect on the inferred percolation transition point for the different reionization scenarios. We deduce the optimal size of the chunks to be cut out of the lightcone maps to estimate the LCS. To do this, a balance has to be struck between a large enough chunk for a robust estimation of the LCS and a small enough chunk to minimize the redshift evolution of the signal along the line of sight.

This work is structured as follows: section 2 describes the simulations of the 21-cm lightcone maps, section 3 outlines the methodology followed for the percolation analysis, and section 4 describes the results of the percolation analysis on lightcone maps. We summarize and conclude the work in section 5. Throughout this work, we use the the Λ CDM cosmology of the WMAP five-year data release: $h = 0.7$, $\Omega_m = 0.27$, $\Omega_\Lambda = 0.73$, $\Omega_b h^2 = 0.0226$.

2 Simulations

2.1 Semi-numerical simulation of reionization

Theoretical modeling of the reionization era requires simulations of high dynamic range in mass and length scales to account for the key physical processes in the sources responsible for reionization at small length scales and also the details of large-scale effects such as evolution of underlying matter density fields, phase change of the IGM, and radiative feedback resulting from the reionization. This requires us to have a simulation of a large cosmological volume and a high resolution.

One way to simulate reionization is to solve the cosmological radiative transfer equation along the path of every heating and ionizing photon [108–112]. These 3D radiative transfer simulations help us study the evolution of the IGM with the progress of reionization, but are computationally very expensive. A computationally less expensive alternative is to use a semi-numerical technique based on the excursion set formalism [2]. This technique compares the number of HI atoms to the number of HI ionizing photons present in a smoothing volume to generate the ionization maps [99, 113]. In this work, we have used the 21-cm differential brightness temperature maps that were generated using the semi-numerical simulation code **Sem-Num** [100, 113]. The semi-numerical simulation used for the analysis in this work is performed using the following steps:

- Initially, the dark matter distribution is generated with an N -body gravity-only simulation at a set of redshifts ranging from 13.2 to 7.2.
- The Spherical overdensity halo finder algorithm is then employed on this dark matter particle distribution to identify the collapsed dark matter halos. These halos are considered to be the hosts of sources that emit ionizing photons.
- Once collapsed halos above a threshold halo mass, hosting the ionizing sources are identified, we model the spectrum of photons emitted from these halos and use the excursion set formalism to generate the ionization field, which is then converted to the 21-cm field.

By following the above procedure, we generate coeval cubes of size $500 h^{-1}$ Mpc (714 Mpc) in length along each side on the comoving scale [99]. The underlying dark matter distribution at each redshift was generated using a P^3M N -body simulation code **CUBEP³M** [114] as part of the **PRACE4LOFAR** project. For the dark matter field, the authors of [99] have used 6912^3 particles of mass $4.0 \times 10^7 M_\odot$ on a 13824^3 mesh (comoving grid resolution of 0.052 Mpc), and later these simulated matter and halo catalogues are interpolated on a 600^3 grid (comoving grid resolution of 1.19 Mpc). The parameters considered for the semi-numerical reionization simulation to generate the brightness temperature maps are minimum halo mass ($M_{h,\min}$), mean free path of photons (R_{mfp}), and the number of ionizing photons entering the IGM per baryon (N_{ion}). The minimum halo mass required to host the luminous sources in these reionization simulations is $M_{h,\min} = 2.09 \times 10^9 M_\odot$, whereas R_{mfp} and N_{ion} are model-dependent and are discussed in the following sections.

2.2 Reionization source models and scenarios

The evolution of the topology of ionized bubbles depends on both the properties of sources emitting ionizing photons and the IGM characteristics. Thus, it is possible to generate topologically distinct ionization fields by varying the source characteristics and properties of the IGM. In this work, we consider four source properties resulting in five different reionization scenarios with different topological evolution of ionized bubbles. These scenarios were distinguished in coeval 21-cm maps in Paper I, and we examine their distinguishability when the lightcone effect is implemented. In the following section, we briefly describe the source models considered in this work, detailed in [99].

2.2.1 Reionization source models

In this work, we consider four different source models based on the type and intensity of photons emitted by them. In the next section, we describe how these source models are combined to generate topologically distinct reionization scenarios.

- **Ultraviolet photons (fiducial model):** In this model, we assume that UV photons emitted from the galaxies residing in collapsed halos are responsible for reionization. It is also assumed that the number of ionizing photons emitted from a luminous galaxy follows the following relation:

$$N_\gamma(M_h) = N_{\text{ion}} \frac{M_h \Omega_b}{m_p \Omega_m}, \quad (2.1)$$

where m_p is the mass of a proton, M_h is the mass of the halo that hosts the source, and N_{ion} is the number of ionizing photons entering the IGM per baryon.

- **Uniform Ionizing Background (UIB photons):** The hard X-rays emitted by sources like X-ray binaries, AGNs, etc, are assumed to be the dominant cause of reionization in this model, and the number of photons emitted by these sources follows the relation 2.1. The X-rays emitted by these sources travel long distances before getting absorbed by the intervening IGM. The long mean free path of hard X-rays will result in a uniform ionizing photon distribution contributing to a uniform ionizing background. This results in an outside-in reionization scenario where low-density regions are ionized first and high-density regions later.

- **Soft X-ray photons (SXR):** In this source model, soft X-ray photons generated using equation 2.1 dominate reionization. These SXRs contribute to a uniform ionizing background limited by the mean free path of photons. The mean free path of SXR photons is dependent on the frequency and redshift of their origin and is determined by following the formalism used in [115]. In this work, we assume that all the SXR photons emitted by the sources have the same energy of 200 eV. The photons emitted are uniformly distributed in a spherical region around the source. The radius of this uniform distribution around the source is determined by the mean free path of SXR photons.
- **Power law mass dependent efficiency (PL):** In this source model, we consider that the number of UV photons emitted by the ionizing source (N_γ) is proportional to the n -th power of the mass of the host dark matter halo (M_h).

$$N_\gamma(M_h) \propto M_h^n, \quad (2.2)$$

In this work, we consider a power law index of 3 in order to generate the differential brightness temperature maps for our analysis.

2.2.2 Reionization Scenarios

In this section, we discuss five different reionization scenarios generated by using the above-mentioned source models. The contribution of source models to different reionization scenarios is summarized in Table 1.

Reionization Scenarios	UV	UIB	SXR	PL,n
Fiducial	100%	-	-	1.0
Clumping	100%	-	-	1.0
PL($n = 3$)	100%	-	-	3.0
UIB dominated	20%	80%	-	1.0
UV+SXR+UIB	50%	10%	40%	1.0

Table 1. Contribution of different source models in our reionization scenarios.

The fiducial, clumping, and $PL(n = 3)$ reionization scenarios assume that only UV photons emitted from the galaxies residing in collapsed halos of mass $\geq 2.09 \times 10^9 M_\odot$ contribute to reionization. The clumping reionization scenario is the only one among these reionization scenarios that assumes density-dependent recombination, whereas in other scenarios, a uniform rate of recombination is taken into account. This realistic non-uniform rate of recombination in the clumping reionization scenario leads to the formation of self-shielded regions with high optical depth, like Lyman limit systems [116, 117], resulting in a topologically distinct 21-cm map. In the $PL(n = 3)$ reionization scenario, the high mass halos have a higher weightage of ionizing UV photon contribution (2.2), resulting in the formation of relatively larger ionized bubbles around the high mass halos. In the other models, like UIB and UV+SXR+UIB, we assume a varied contribution of ionizing photons from different source models as mentioned in Table 1. As the name suggests, the dominant contribution of hard X-rays to reionization leads to the formation of a uniform ionizing background in the UIB model. The UV+SXR+UIB model takes into account the contribution of three source models, making UV, Hard X-ray, and soft X-ray photons generate the ionization field.

The proportionality constant N_{ion} was tuned in the reionization scenarios considered (Table 1) such that they follow the same reionization history, i.e., they have the same mass-averaged neutral fraction at a given redshift. Note that these reionization scenarios lead to distinct reionization topologies, and we study the evolution of their topology using percolation analysis.

2.3 Simulating lightcone maps

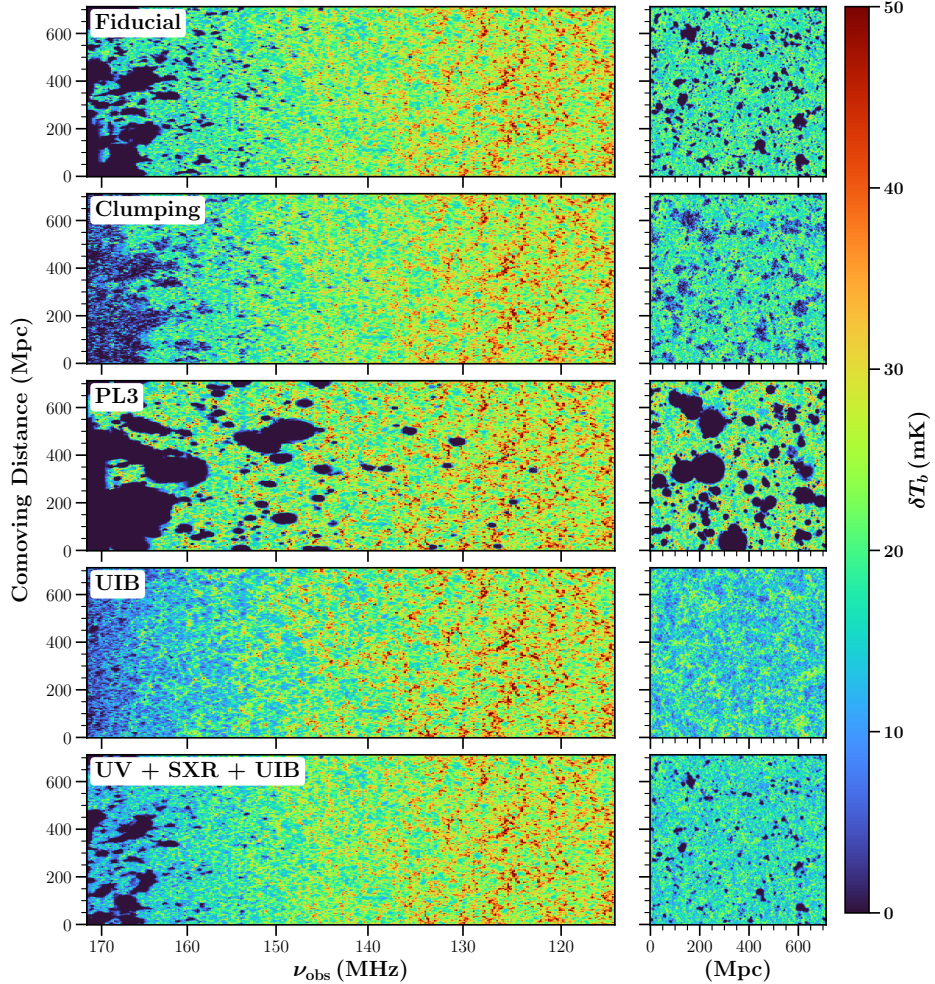


Figure 1. *Left:* Corresponding slices cut along the line of sight of the 21-cm brightness temperature lightcone maps for the fiducial, clumping, PL3, UIB, and UV+SXR+UIB reionization scenarios. The horizontal axis is the line of sight with reionization progressing from right to left. The observed frequencies ν_{obs} correspond to the frequencies at which the 21-cm emission from the redshift of the slice can be observed. *Right:* Corresponding slices of the same lightcone maps cut perpendicular to the line of sight at $z = 7.91$.

By following the procedure mentioned in the above sections, we generated coeval maps at redshifts ranging from 13.2 to 7.2 for each reionization scenario. We briefly mention the procedure to generate lightcone maps from coeval maps here. Note that the above-mentioned formalism is similar to the one employed in [101].

- We prepare a redshift list Z with entries $z_1, z_2, z_3, \dots, z_N$ ($z_1 < z_2 < z_3 \dots < z_N$) with $N = L/l$, where L is co-moving distance between lowest (z_1) and highest (z_N) redshifts in the generated coeval boxes and l is the grid spacing in the coeval maps.
- To construct the p th slice of a lightcone (z_p) using the coeval cubes containing M slices, we first compute the remainder q of the integer division $\frac{p}{M}$. We then take the q th slice from the coeval cubes at z_l and z_{l+1} such that $z_l \leq z_p \leq z_{l+1}$ and use linear interpolation to construct the p th slice of the lightcone.

Once the lightcone maps are generated following the above-mentioned approach for each reionization scenario, we relabel the line of sight axis with the observed frequency (ν_{obs}) in these maps using

$$\nu_{\text{obs}} = \frac{1420}{1+z} \text{ MHz}, \quad (2.3)$$

where z is the redshift of the slice we consider and 1420 MHz is the rest-frame frequency of 21-cm line emission.

3 Methodology

3.1 Percolation analysis

The first luminous sources, once formed ($z \approx 15$), emit X-ray and UV photons, which heat and subsequently ionize the neutral Hydrogen present in the intergalactic medium (IGM). As this process of reionization progresses, new ionized regions start forming, and existing ionized regions grow and overlap with each other. As time progresses, these ionized regions get interconnected to form a single large ionized region extending throughout the IGM. This phase transition, resulting in the formation of a single LIR, is called the percolation transition [23–25, 96, 98].

In this work, we use the Largest Cluster Statistic (LCS) [7, 23, 25, 95, 96, 98] to track the percolation process in lightcone maps and determine the timing of percolation transition in different reionization scenarios. LCS gives a measure of the fraction of ionized volume present in the LIR and is defined as follows:

$$\text{LCS} = \frac{\text{Volume of the largest ionized region}}{\text{Total volume of all the ionized regions}}. \quad (3.1)$$

The Filling Factor (FF) is another statistic used to probe the ionization state of the IGM. FF gives a measure of the fraction of the ionized volume present in the simulation volume considered and is defined as follows:

$$\text{FF} = \frac{\text{Total ionization volume}}{\text{Volume of the simulation box}}. \quad (3.2)$$

After percolation, the entire ionized volume is carried by the LIR, extending from one end of the simulation box to the other, resulting in an LCS of 1. The FF is the volume-averaged ionized fraction, which helps us determine the evolution of the ionization state of the IGM during reionization.

To compute the LCS and FF in a given tomographic volume, we use the SURFGEN2 algorithm, whose detailed description can be found in [23, 24, 118]. SURFGEN2 binarizes the given tomographic volume based on a threshold value and identifies the ionized regions

by the Friends-of-Friends (FoF) algorithm. Once the ionized regions are identified, their Shapefinders [80] are computed using the `Marching Cubes 33` algorithm [119], and the values of LCS and FF are also calculated. Note that `SURFGEN2` counts only fully ionized cells while computing cluster statistics.

3.2 Calculating LCS in lightcone maps

When `SURFGEN2` is employed on a lightcone map, it outputs a single value of LCS corresponding to that map, with which one cannot understand the evolution of LCS with observed frequency and hence redshift. In order to understand the evolution of the cluster statistics, we divide lightcone maps into subvolumes by using a moving volume approach as illustrated in Figure 2. We choose a subvolume (called a moving volume) of fixed frequency width along the line of sight and move it along the line of sight by one simulation grid unit at a time, starting from the highest observed frequency. We then compute cluster statistics using `SURFGEN2` in the subvolume corresponding to the location of the moving volume at each step. The cluster statistics are then labeled with the mean observed frequency at that step. By following this approach, we compute the evolution of cluster statistics in a lightcone map as discussed in section 4.

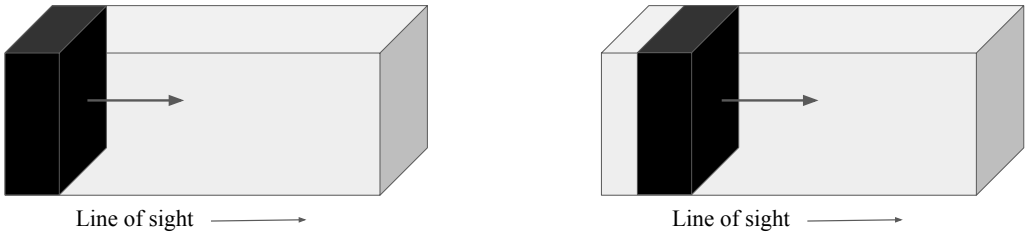


Figure 2. This figure illustrates the moving volume approach with the lightcone represented as a grey solid box and the moving volume represented as a black solid box. The figure on the left-hand side represents the first iteration, and the figure on the right-hand side represents the second iteration, where the moving volume is moved by one grid unit.

4 Results

4.1 Percolation analysis on coeval maps

The percolation behavior of the ionized bubbles in the coeval maps has been extensively studied in earlier works, including papers I, IIa, and IIb. In this subsection, we summarize the results from these works before discussing the results from this paper.

- A sharp increase in the value of LCS has been observed at the onset of percolation in all the reionization scenarios considered from Table 1. The redshift (or observed frequency) at which this percolation transition occurs depends on the reionization scenario, indicating the strong dependence on the 21-cm topology and can be used to distinguish different reionization source models [25].
- Among the reionization scenarios considered, the ionized bubbles of the clumping model of the coeval maps percolate at the earliest stages and the UIB model at the most

advanced stages of reionization. Additionally, the number of interconnections among the ionized regions, determined by genus, is much higher in the clumping scenario due to the formation of neutral islands that tunnel through the ionized regions [25].

- The system noise and the effect of SKA-Low synthesized beam introduce a bias in determining the onset of percolation. The robust recovery of the reionization history requires a minimum of 2000 hrs of observation to suppress the thermal noise, and a post-calibration antenna-based gain error tolerance of approximately 0.02% to prevent artificial fragmentation of the largest ionized region [96, 98].

The analyses summarized above were primarily conducted using coeval boxes. In this work, we extend this study by applying percolation analysis to lightcone maps, presented in the subsequent sections.

4.2 Percolation analysis on fiducial lightcone map

The percolation transition, characterized by a steep rise in the LCS, can be estimated by tracking the evolution of the LIR within a simulation box. In this work, we employ a moving volume approach to track the evolution of the LIR in lightcone tomographic maps and compare it with its coeval counterpart for each reionization scenario to understand the bias introduced in the timing of percolation when the lightcone effect is considered. The subvolumes generated using the moving volume approach in this work are chunks of the lightcone map whose frequency width depends on the size of the moving volume chosen to generate them. To understand the impact of the size of moving volume, we perform this analysis by varying it from 3 MHz to 15 MHz in steps of 3 MHz along the line of sight in lightcone maps. The LCS and FF are calculated in all these subvolumes following the procedure mentioned in section 3.2. In the case of coeval maps, we compute the LCS and FF for the entire map at a particular frequency (redshift). In Figure 3, we present the evolution of LCS with observed frequency in the fiducial lightcone map for different moving volume sizes along with its coeval counterpart.

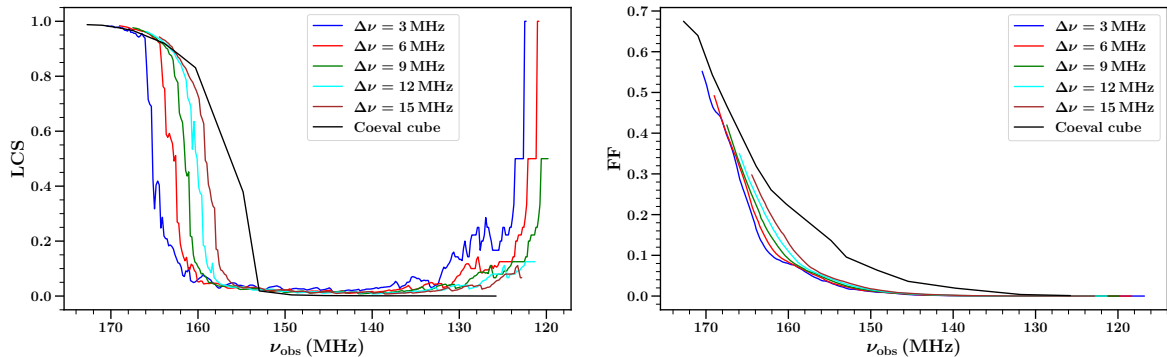


Figure 3. Evolution of the LCS (left) and FF (right) of moving volumes of different spectral bandwidths $\Delta\nu$ with their observed central frequency ν_{obs} for the fiducial 21-cm lightcone.

We observe that each moving volume size exhibits a characteristic shape in the evolution of LCS. As the moving volume size increases, the mean observed frequency used to label it assumes a lower value, resulting in a bias in the timing of percolation onset. As a result, it appears that the onset of percolation started at an earlier stage of reionization (lower

observed frequency) with an increase in the moving volume size. Additionally, LCS assumes a relatively high value for smaller moving volume sizes in lightcone maps at lower observed frequencies (beginning of the reionization) when compared to the LCS in coeval maps at that stage. This high value of LCS does not indicate the percolation of ionized bubbles, which is observed at later stages. Instead, it is attributed to the formation of small ionized bubbles at the beginning of reionization, among which the largest bubble occupies a very large fraction of the total ionized volume in the subvolume chosen at that frequency for the analysis. As we increase the size of the moving volume, the subvolume chosen at that frequency accommodates more ionized bubbles in the chunk, thereby reducing the value of LCS. This high value of LCS at lower observed frequencies is not observed in coeval maps, as the large size of these maps accounts for a large number of ionized bubbles, resulting in a decrease in the fraction of ionized volume occupied by the LIR.

As the moving volume moves towards later stages of reionization, the formation of new ionized bubbles in the subvolumes used to compute the percolation statistics leads to an increase in the ionization volume. This results in a steep fall in LCS for low moving volume sizes. At the onset of percolation, ionized bubbles begin to coalesce, and the volume fraction occupied by the LIR increases rapidly, approaching unity. FF increases with observed frequency for all moving volume sizes considered, indicating an increase in ionization volume or the progression of reionization with time within the subvolumes of the lightcone map. We find that the FF estimated using the moving volume approach is lower than the FF calculated in coeval maps, which is attributed to small but finite frequency evolution within the chunk. This increase in FF for all moving volume sizes is observed to be consistent for all the reionization scenarios we discuss in the next section.

4.3 Evolution of LIR in different reionization scenarios

In this section, we discuss the evolution of the largest ionized region using moving volume sizes of 3 MHz, 9 MHz, and 15 MHz on lightcone maps of different reionization scenarios described in Table 1. The reionization scenarios considered in this work take into account different source properties and characteristics of the IGM, resulting in distinct topological evolution of HII bubbles. Figure 4 shows the evolution of LCS with observed frequency in lightcones of the different reionization scenarios considered, with the onset of percolation in corresponding coeval maps represented by vertical lines. As shown in Figure 4, each reionization scenario has a particular characteristic shape in the evolution of LCS with observed frequency indicating the percolation transition occurring at different observed frequencies. Additionally, the percolation transition shifts to lower observed frequencies with increasing moving volume size, similar to the fiducial model. The high fluctuations for smaller moving volume sizes are attributed to the lack of a sufficient number of ionized regions for a statistically significant estimation of LCS, and discontinuity of interconnections in the subvolumes generated using the moving volume approach. As we increase the size of the subvolume, we account for an increasing number of interconnections, and it is reflected in the relatively smooth evolution of LCS.

Among all the reionization scenarios, the clumping model shows a high degree of offset in the timing of percolation when compared to its coeval counterpart. The clumping model has similar source properties as those of the fiducial model, but different IGM characteristics, resulting in the formation of isolated neutral regions due to a non-uniform rate of recombination. These isolated HI regions lead to an increased number of tunnels in the ionization topology, with multiply connected ionized regions characterized by high genus values (see

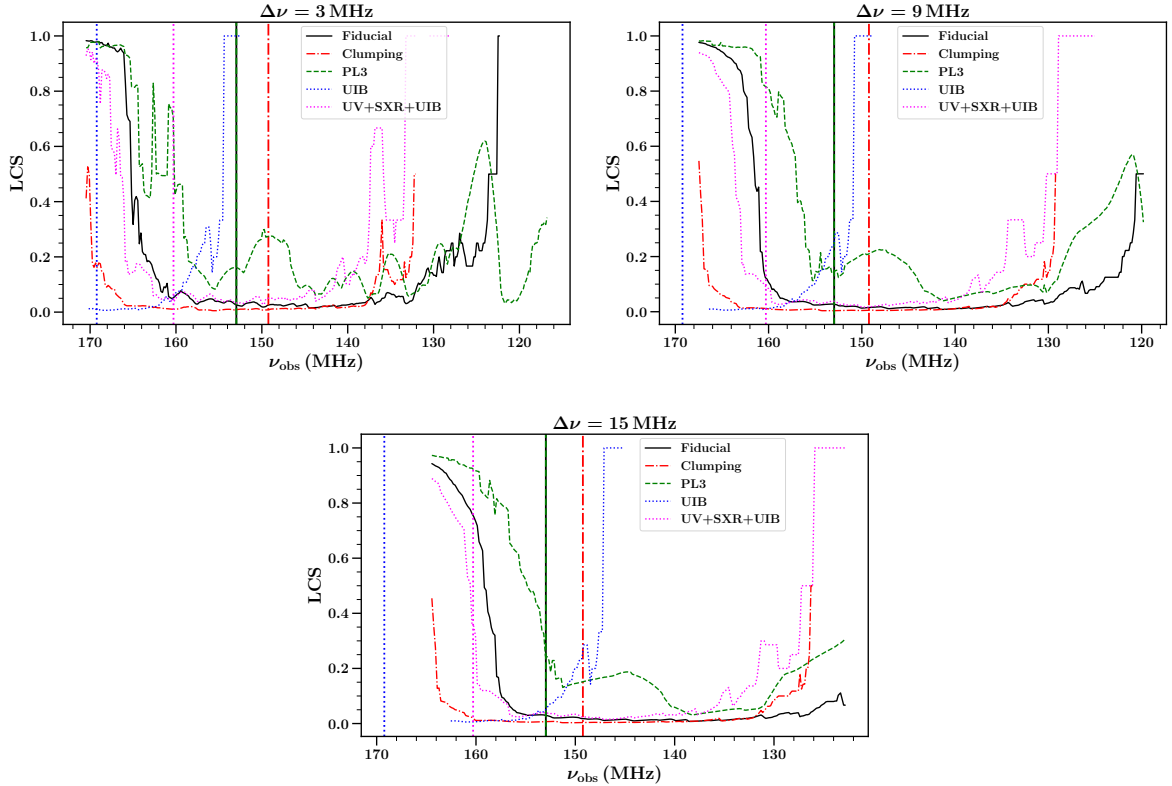


Figure 4. Evolution of the LCS of moving volumes with their observed central frequency ν_{obs} along lightcones of different reionization scenarios at spectral bandwidths $\Delta\nu = 3$ MHz (top left), 9 MHz (top right), and 15 MHz (bottom). The vertical lines denote the observed frequency at which percolation transition occurs for the coeval 21-cm map of the corresponding reionization scenario.

Figure 7, Paper I). The subvolumes that are generated using the moving volume approach in the clumping model do not account for all the interconnections between ionized bubbles due to their limited size. This results in a smaller LIR disconnected from other ionized bubbles, which is reflected in the lower value of LCS. However, the coeval volume of the clumping model accounts for the interconnections comparable to the length of the simulation box between ionized bubbles, resulting in percolation at very low observed frequencies. The onset of percolation in the clumping lightcone map is observed at higher frequencies for all the moving volume sizes when the ionization volume increases significantly to connect the isolated ionized bubbles in the subvolume.

In the case of the PL($n = 3$) model, the number of ionizing photons emitted by the sources residing in high mass halos is much higher when compared to the other models, resulting in the formation of very large ionized bubbles around the source. As the lightcone map captures the spatial and temporal evolution of the 21-cm signal, each subvolume chosen to compute the LCS has a different mass distribution of halos, resulting in the formation of LIR at different locations as reionization progresses (see Figure 5). This results in a change in the LIR accounted to compute LCS with observed frequency in subvolumes until the onset of percolation, reflected in the high variance in its evolution compared to other models. The model also exhibits bias in the observed onset of percolation at 3 MHz and 9 MHz moving volume sizes, similar to that of the fiducial and clumping models. The timing of percolation

for the 15 MHz moving volume size closely matches the coeval case.

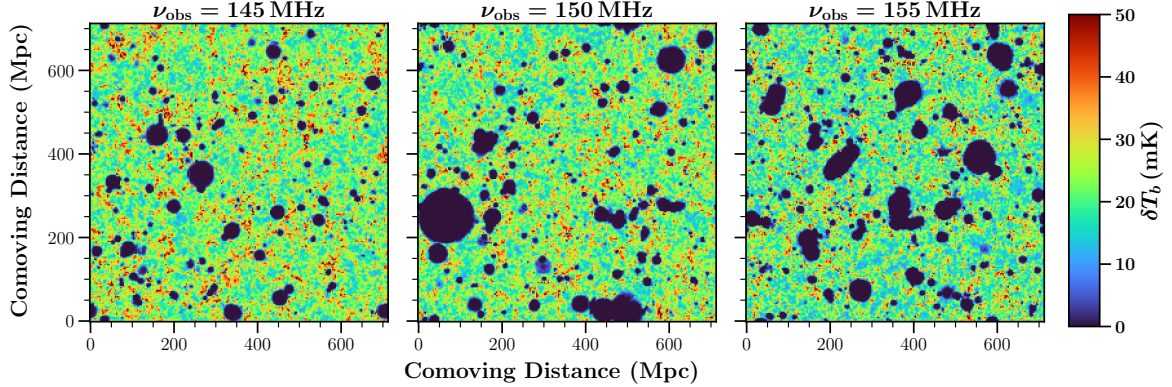


Figure 5. Slices of the $PL(n = 3)$ model lightcone perpendicular to the line of sight at $\nu_{\text{obs}} = 145$ MHz, 150 MHz, and 155 MHz.

Unlike the models discussed above, the UIB model does not exhibit percolation in the frequency range of the lightcone considered. In the UIB model, reionization is dominated by hard X-rays, leading to an outside-in reionization resulting in a uniform background of ionization. Percolation in the coeval cube of the UIB model happens at an advanced stage of reionization compared to other reionization scenarios considered. Although the moving volume approach covers the frequency range corresponding to the onset of percolation in its coeval counterpart, it does not account for the rapid rise of interconnections at that frequency due to its limited size.

The UV+SXR+UIB model takes into account both inside-out and outside-in reionization processes. In this model, like in other models, the onset of percolation is determined by the size of the moving volume chosen to do the analysis. Among all the models considered, the lightcone of the UV+SXR+UIB model exhibits the least bias in determining the timing of the onset of percolation in comparison to its coeval maps.

5 Summary

The progression of reionization of HI gas in the intergalactic medium and the sources of ionizing photons that led to it are not well understood to date. Possible sources of reionization include UV radiation from young stars within galaxies, hard X-rays emitted by AGNs that form a uniform ionizing background, soft X-ray photons originating from high-redshift starburst galaxies, X-ray binaries, etc. The relation between the rate of emission of ionizing photons by a source and its host halo mass is also not well understood, and there can be multiple possible relations between the two quantities. Additionally, the rate of recombination of HII is expected to be density dependent. All these above factors lead to multiple different reionization scenarios, of which we studied five scenarios as detailed in 2.2.2.

In order to interpret tomographic 21-cm intensity maps from the EoR and test the plausibility of the different reionization scenarios, the signal needs to be forward modeled and compared with observations. For this, summary statistics that both reduce the dimensionality of the data and, at the same time, capture key information of the signal are needed. Image-based statistics, such as LCS, are helpful for this purpose, as they capture the topological information of ionized regions. The ability of LCS to distinguish between these scenarios

based on the timing of their percolation transition (the stage at which LCS rises sharply towards unity) was studied in detail in Paper I. In this work, we have extended this analysis to more realistic observations by incorporating the lightcone effect into our simulations, which is inherent to intensity mapping experiments over a wide frequency (redshift) range.

Estimating the LCS of a 21-cm lightcone would yield a single value, washing out the information of its redshift evolution, and hence the percolation transition. In order to capture the redshift evolution of LCS, a lightcone must be divided into subvolumes, and the LCS must be computed on these subvolumes to characterize its evolution. The subvolume must be small enough such that the LCS is not averaged over a wide redshift range. At the same time, it must be large enough so that it accommodates a large number of ionized regions, and the computed LCS value is statistically significant. Dividing the lightcone into such disjoint subvolumes would give a small number of them, and the redshift evolution of LCS would not be sampled effectively. We therefore employed a moving volume approach where the subvolume translates along the lightcone as described in [3.2](#).

We found that choosing subvolumes with lower spectral bandwidth delays percolation compared to a coeval cube. The evolution of the filling factor is similar across different moving volumes and differs from the coeval case due to redshift evolution of the signal within a moving volume. The onset of percolation for all the reionization scenarios considered depends upon the size of the moving volume chosen to compute the LCS. As we increase the size of the moving volume, the timing of the onset of percolation approaches that of its coeval counterpart. For the moving volume size of 15 MHz, the percolation transition in the PL ($n = 3$) and UV+SXR+UIB models matches that of their coeval counterparts, making it the optimal chunk size for these models.

Acknowledgments

The authors would like to acknowledge useful discussions with Ilian T. Iliev regarding this work. MMD, SM and AD thank the Science and Engineering Research Board (SERB) and the Department of Science and Technology (DST), Government of India, for financial support through Core Research Grant No. CRG/2021/004025 titled “Observing the Cosmic Dawn in Multicolor using Next Generation Telescopes”. CSM would like to acknowledge financial support from the Council of Scientific and Industrial Research (CSIR) via a CSIR-SRF Fellowship (Grant No. 09/1022(0080)/2019-EMR-I) and from the ARCO Prize Fellowship. SKP acknowledge the financial support by the Department of Science and Technology, Government of India, through the INSPIRE Fellowship [IF200312]. LN acknowledge the financial support by the Department of Science and Technology, Government of India, through the INSPIRE Fellowship [IF210392]

References

- [1] R. Barkana and A. Loeb, *In the beginning: the first sources of light and the reionization of the universe*, *Physics Reports* **349** (2001) 125.
- [2] S.R. Furlanetto, M. Zaldarriaga and L. Hernquist, *The growth of $h\ ii$ regions during reionization*, *The Astrophysical Journal* **613** (2004) 1.
- [3] I.T. Iliev, G. Mellema, U.-L. Pen, H. Merz, P.R. Shapiro and M.A. Alvarez, *Simulating cosmic reionization at large scales – i. the geometry of reionization*, *Monthly Notices of the Royal Astronomical Society* **369** (2006) 1625.

[4] B.E. Robertson, R.S. Ellis, J.S. Dunlop, R.J. McLure and D.P. Stark, *Early star-forming galaxies and the reionization of the Universe*, *Nature* **468** (2010) 49 [[1011.0727](#)].

[5] P. Dayal and A. Ferrara, *Early galaxy formation and its large-scale effects*, *Physics Reports* **780-782** (2018) 1.

[6] Planck Collaboration, P.A.R. Ade, N. Aghanim, C. Armitage-Caplan, M. Arnaud, M. Ashdown et al., *Planck 2013 results. XVI. Cosmological parameters*, *Astronomy & Astrophysics* **571** (2014) A16 [[1303.5076](#)].

[7] S. Bharadwaj, V. Sahni, B.S. Sathyaprakash, S.F. Shandarin and C. Yess, *Evidence for filamentarity in the las campanas redshift survey*, *The Astrophysical Journal* **528** (2000) 21.

[8] D.J. Croton, P. Norberg, E. Gaztañaga and C.M. Baugh, *Statistical analysis of galaxy surveys – iii. the non-linear clustering of red and blue galaxies in the 2dfgrs*, *Monthly Notices of the Royal Astronomical Society* **379** (2007) 1562.

[9] C.M. Simpson, G.L. Bryan, K.V. Johnston, B.D. Smith, M.-M. Mac Low, S. Sharma et al., *The effect of feedback and reionization on star formation in low-mass dwarf galaxy haloes*, *Monthly Notices of the Royal Astronomical Society* **432** (2013) 1989.

[10] A. Hutter, P. Dayal, G. Yepes, S. Gottlöber, L. Legrand and G. Ucci, *Astraeus i: the interplay between galaxy formation and reionization*, *Monthly Notices of the Royal Astronomical Society* **503** (2021) 3698.

[11] A. Hutter, P. Dayal, L. Legrand, S. Gottlöber and G. Yepes, *Astraeus – iii. the environment and physical properties of reionization sources*, *Monthly Notices of the Royal Astronomical Society* **506** (2021) 215.

[12] X. Fan, M.A. Strauss, R.H. Becker, R.L. White, J.E. Gunn, G.R. Knapp et al., *Constraining the Evolution of the Ionizing Background and the Epoch of Reionization with $z \sim 6$ Quasars. II. A Sample of 19 Quasars*, *The Astronomical Journal* **132** (2006) 117 [[astro-ph/0512082](#)].

[13] G.D. Becker, J.S. Bolton, P. Madau, M. Pettini, E.V. Ryan-Weber and B.P. Venemans, *Evidence of patchy hydrogen reionization from an extreme $\text{Ly}\alpha$ trough below redshift six*, *Monthly Notices of the Royal Astronomical Society* **447** (2015) 3402.

[14] E. Bañados, B.P. Venemans, C. Mazzucchelli, E.P. Farina, F. Walter, F. Wang et al., *An 800-million-solar-mass black hole in a significantly neutral Universe at a redshift of 7.5*, *Nature Astronomy* **553** (2018) 473 [[1712.01860](#)].

[15] Planck Collaboration, N. Aghanim, Y. Akrami, M. Ashdown, J. Aumont, C. Baccigalupi et al., *Planck 2018 results. VI. Cosmological parameters*, *Astronomy & Astrophysics* **641** (2020) A6 [[1807.06209](#)].

[16] E.M. Hu, L.L. Cowie, A.J. Barger, P. Capak, Y. Kakazu and L. Trouille, *An atlas of $z = 5.7$ and $z = 6.5$ $\text{Ly}\alpha$ emitters**, *The Astrophysical Journal* **725** (2010) 394.

[17] A.M. Morales, C.A. Mason, S. Bruton, M. Gronke, F. Haardt and C. Scarlata, *The evolution of the lyman-alpha luminosity function during reionization*, *The Astrophysical Journal* **919** (2021) 120.

[18] M. Tang, D.P. Stark, Z. Chen, C. Mason, M. Topping, R. Endsley et al., *Jwst/nirspec spectroscopy of $z = 7-9$ star-forming galaxies with ceers: new insight into bright $\text{Ly}\alpha$ emitters in ionized bubbles*, *Monthly Notices of the Royal Astronomical Society* **526** (2023) 1657.

[19] C. Witten, N. Laporte, S. Martin-Alvarez, D. Sijacki, Y. Yuan, M.G. Haehnelt et al., *Deciphering Lyman- α emission deep into the epoch of reionization*, *Nature Astronomy* **8** (2024) 384 [[2303.16225](#)].

[20] P. Madau, A. Meiksin and M.J. Rees, *21 Centimeter Tomography of the Intergalactic Medium at High Redshift*, *The Astrophysical Journal* **475** (1997) 429 [[astro-ph/9608010](#)].

[21] S. Zaroubi, *The Epoch of Reionization*, in *The First Galaxies*, T. Wiklind, B. Mobasher and V. Bromm, eds., vol. 396 of *Astrophysics and Space Science Library*, p. 45, Jan., 2013, DOI [\[1206.0267\]](#).

[22] G. Mellema, L. Koopmans, H. Shukla, K.K. Datta, A. Mesinger and S. Majumdar, *HI tomographic imaging of the Cosmic Dawn and Epoch of Reionization with SKA*, in *Advancing Astrophysics with the Square Kilometre Array (AASKA14)*, p. 10, Apr., 2015, DOI [\[1501.04203\]](#).

[23] S. Bag, R. Mondal, P. Sarkar, S. Bharadwaj and V. Sahni, *The shape and size distribution of hii regions near the percolation transition*, *Monthly Notices of the Royal Astronomical Society* **477** (2018) 1984.

[24] S. Bag, R. Mondal, P. Sarkar, S. Bharadwaj, T.R. Choudhury and V. Sahni, *Studying the morphology of hi isodensity surfaces during reionization using shapefinders and percolation analysis*, *Monthly Notices of the Royal Astronomical Society* **485** (2019) 2235.

[25] A. Pathak, S. Bag, S. Dasgupta, S. Majumdar, R. Mondal, M. Kamran et al., *Distinguishing reionization models using the largest cluster statistics of the 21-cm maps*, *Journal of Cosmology and Astroparticle Physics* **2022** (2022) 027.

[26] S. Bharadwaj and S. Saiyad Ali, *On using visibility correlations to probe the hi distribution from the dark ages to the present epoch – i. formalism and the expected signal*, *Monthly Notices of the Royal Astronomical Society* **356** (2005) 1519.

[27] V. Jelić, S. Zaroubi, P. Labropoulos, R.M. Thomas, G. Bernardi, M.A. Brentjens et al., *Foreground simulations for the lofar-epoch of reionization experiment*, *Monthly Notices of the Royal Astronomical Society* **389** (2008) 1319.

[28] V. Jelić, S. Zaroubi, P. Labropoulos, G. Bernardi, A.G. de Bruyn and L.V.E. Koopmans, *Realistic simulations of the galactic polarized foreground: consequences for 21-cm reionization detection experiments*, *Monthly Notices of the Royal Astronomical Society* **409** (2010) 1647.

[29] O. Zahn, A. Mesinger, M. McQuinn, H. Trac, R. Cen and L.E. Hernquist, *Comparison of reionization models: radiative transfer simulations and approximate, seminumeric models*, *Monthly Notices of the Royal Astronomical Society* **414** (2011) 727.

[30] S. Choudhuri, S. Bharadwaj, S.S. Ali, N. Roy, H.T. Intema and A. Ghosh, *The angular power spectrum measurement of the galactic synchrotron emission in two fields of the tgss survey*, *Monthly Notices of the Royal Astronomical Society: Letters* **470** (2017) L11.

[31] A. Chakraborty, N. Roy, A. Datta, S. Choudhuri, K.K. Datta, P. Dutta et al., *Detailed study of elais n1 field with the ugmrt – ii. source properties and spectral variation of foreground power spectrum from 300–500 mhz observations*, *Monthly Notices of the Royal Astronomical Society* **490** (2019) 243.

[32] A. Mazumder, A. Chakraborty, A. Datta, S. Choudhuri, N. Roy, Y. Wadadekar et al., *Characterizing eor foregrounds: a study of the lockman hole region at 325 mhz*, *Monthly Notices of the Royal Astronomical Society* **495** (2020) 4071.

[33] N. Barry, B. Hazelton, I. Sullivan, M.F. Morales and J.C. Pober, *Calibration requirements for detecting the 21 cm epoch of reionization power spectrum and implications for the ska*, *Monthly Notices of the Royal Astronomical Society* **461** (2016) 3135.

[34] A.H. Patil, S. Yatawatta, S. Zaroubi, L.V.E. Koopmans, A.G. de Bruyn, V. Jelić et al., *Systematic biases in low-frequency radio interferometric data due to calibration: the lofar-eor case*, *Monthly Notices of the Royal Astronomical Society* **463** (2016) 4317.

[35] A. Ewall-Wice, J.S. Dillon, A. Liu and J. Hewitt, *The impact of modelling errors on interferometer calibration for 21 cm power spectra*, *Monthly Notices of the Royal Astronomical Society* **470** (2017) 1849.

[36] A. Mazumder, A. Datta, A. Chakraborty and S. Majumdar, *Observing the reionization: effect of calibration and position errors on realistic observation conditions*, *Monthly Notices of the Royal Astronomical Society* **515** (2022) 4020.

[37] C.H. Jordan, S. Murray, C.M. Trott, R.B. Wayth, D.A. Mitchell, M. Rahimi et al., *Characterization of the ionosphere above the murchison radio observatory using the murchison widefield array*, *Monthly Notices of the Royal Astronomical Society* **471** (2017) 3974.

[38] C.M. Trott, C.H. Jordan, S.G. Murray, B. Pindor, D.A. Mitchell, R.B. Wayth et al., *Assessment of ionospheric activity tolerances for epoch of reionization science with the murchison widefield array*, *The Astrophysical Journal* **867** (2018) 15.

[39] S.K. Pal, A. Datta and A. Mazumder, *Ionospheric effect on the synthetic epoch of reionization observations with the ska1-low*, *Journal of Cosmology and Astroparticle Physics* **2025** (2025) 058.

[40] N.S. Kern, A.R. Parsons, J.S. Dillon, A.E. Lanman, N. Fagnoni and E. de Lera Acedo, *Mitigating internal instrument coupling for 21 cm cosmology. i. temporal and spectral modeling in simulations*, *The Astrophysical Journal* **884** (2019) 105.

[41] G. Paciga, J.G. Albert, K. Bandura, T.-C. Chang, Y. Gupta, C. Hirata et al., *A simulation-calibrated limit on the $h\ i$ power spectrum from the gmrt epoch of reionization experiment*, *Monthly Notices of the Royal Astronomical Society* **433** (2013) 639.

[42] A.R. Parsons, A. Liu, J.E. Aguirre, Z.S. Ali, R.F. Bradley, C.L. Carilli et al., *New Limits on 21 cm Epoch of Reionization from PAPER-32 Consistent with an X-Ray Heated Intergalactic Medium at $z = 7.7$* , *The Astrophysical Journal* **788** (2014) 106 [[1304.4991](#)].

[43] Z.S. Ali, A.R. Parsons, H. Zheng, J.C. Pober, A. Liu, J.E. Aguirre et al., *PAPER-64 Constraints on Reionization: The 21 cm Power Spectrum at $z = 8.4$* , *The Astrophysical Journal* **809** (2015) 61 [[1502.06016](#)].

[44] A.H. Patil, S. Yatawatta, L.V.E. Koopmans, A.G. de Bruyn, M.A. Brentjens, S. Zaroubi et al., *Upper Limits on the 21 cm Epoch of Reionization Power Spectrum from One Night with LOFAR*, *The Astrophysical Journal* **838** (2017) 65 [[1702.08679](#)].

[45] F.G. Mertens, M. Mevius, L.V.E. Koopmans, A.R. Offringa, G. Mellema, S. Zaroubi et al., *Improved upper limits on the 21 cm signal power spectrum of neutral hydrogen at $z \approx 9.1$ from LOFAR*, *Monthly Notices of the Royal Astronomical Society* **493** (2020) 1662 [[2002.07196](#)].

[46] A. Acharya, F. Mertens, B. Ciardi, R. Ghara, L.V.E. Koopmans and S. Zaroubi, *Revised lofar upper limits on the 21-cm signal power spectrum at $z \approx 9.1$ using machine learning and gaussian process regression*, *Monthly Notices of the Royal Astronomical Society: Letters* **534** (2024) L30.

[47] Mertens, F. G., Mevius, M., Koopmans, L. V. E., Offringa, A. R., Zaroubi, S., Acharya, A. et al., *Deeper multi-redshift upper limits on the epoch of reionisation 21 cm signal power spectrum from lofar between $z = 8.3$ and $z = 10.1$* , *Astronomy & Astrophysics* **698** (2025) A186.

[48] N. Barry, M. Wilensky, C.M. Trott, B. Pindor, A.P. Beardsley, B.J. Hazelton et al., *Improving the epoch of reionization power spectrum results from murchison widefield array season 1 observations*, *The Astrophysical Journal* **884** (2019) 1.

[49] C.M. Trott, C.H. Jordan, S. Midgley, N. Barry, B. Greig, B. Pindor et al., *Deep multiredshift limits on Epoch of Reionization 21 cm power spectra from four seasons of Murchison Widefield Array observations*, *Monthly Notices of the Royal Astronomical Society* **493** (2020) 4711 [[2002.02575](#)].

[50] C.D. Nunhokee, D. Null, C.M. Trott, N. Barry, Y. Qin, R.B. Wayth et al., *Limits on the 21 cm power spectrum at $z = 6.5-7.0$ from murchison widefield array observations*, *The Astrophysical Journal* **989** (2025) 57.

[51] HERA Collaboration, Z. Abdurashidova, T. Adams, J.E. Aguirre, P. Alexander, Z.S. Ali et al., *Improved Constraints on the 21 cm EoR Power Spectrum and the X-Ray Heating of the IGM with HERA Phase I Observations*, *The Astrophysical Journal* **945** (2023) 124 [[2210.04912](#)].

[52] R. Ghara, S.K. Giri, G. Mellema, B. Ciardi, S. Zaroubi, I.T. Iliev et al., *Constraining the intergalactic medium at $z \approx 9.1$ using LOFAR Epoch of Reionization observations*, *Monthly Notices of the Royal Astronomical Society* **493** (2020) 4728 [[2002.07195](#)].

[53] R. Mondal, A. Fialkov, C. Fling, I.T. Iliev, R. Barkana, B. Ciardi et al., *Tight constraints on the excess radio background at $z = 9.1$ from LOFAR*, *Monthly Notices of the Royal Astronomical Society* **498** (2020) 4178 [[2004.00678](#)].

[54] B. Greig, A. Mesinger, L.V.E. Koopmans, B. Ciardi, G. Mellema, S. Zaroubi et al., *Interpreting LOFAR 21-cm signal upper limits at $z \approx 9.1$ in the context of high- z galaxy and reionization observations*, *Monthly Notices of the Royal Astronomical Society* **501** (2021) 1 [[2006.03203](#)].

[55] Z. Abdurashidova, J.E. Aguirre, P. Alexander, Z.S. Ali, Y. Balfour, R. Barkana et al., *HERA Phase I Limits on the Cosmic 21 cm Signal: Constraints on Astrophysics and Cosmology during the Epoch of Reionization*, *The Astrophysical Journal* **924** (2022) 51 [[2108.07282](#)].

[56] S.S. Gill, S. Bharadwaj, K.M.A. Elahi, S.K. Sethi and A.K. Patwa, *The EoR 21-cm Bispectrum at $z = 8.2$ from MWA data I: Foregrounds and preliminary upper limits*, *arXiv e-prints* (2025) arXiv:2507.04964 [[2507.04964](#)].

[57] G. Mellema, L.V.E. Koopmans, F.A. Abdalla, G. Bernardi, B. Ciardi, S. Daiboo et al., *Reionization and the Cosmic Dawn with the Square Kilometre Array*, *Experimental Astronomy* **36** (2013) 235 [[1210.0197](#)].

[58] L. Koopmans, J. Pritchard, G. Mellema, J. Aguirre, K. Ahn, R. Barkana et al., *The Cosmic Dawn and Epoch of Reionisation with SKA*, *PoS AASKA14* (2015) 001.

[59] R. Ghara, T.R. Choudhury, K.K. Datta and S. Choudhuri, *Imaging the redshifted 21 cm pattern around the first sources during the cosmic dawn using the SKA*, *Monthly Notices of the Royal Astronomical Society* **464** (2017) 2234 [[1607.02779](#)].

[60] C.J. Schmit and J.R. Pritchard, *Emulation of reionization simulations for bayesian inference of astrophysics parameters using neural networks*, *Monthly Notices of the Royal Astronomical Society* **475** (2017) 1213.

[61] D. Prelogović, A. Mesinger, S. Murray, G. Fiameni and N. Gillet, *Machine learning astrophysics from 21 cm lightcones: impact of network architectures and signal contamination*, *Monthly Notices of the Royal Astronomical Society* **509** (2021) 3852.

[62] H. Tiwari, A.K. Shaw, S. Majumdar, M. Kamran and M. Choudhury, *Improving constraints on the reionization parameters using 21-cm bispectrum*, *Journal of Cosmology and Astroparticle Physics* **2022** (2022) 045.

[63] D. Breitman, A. Mesinger, S.G. Murray, D. Prelogović, Y. Qin and R. Trotta, *21cmemu: an emulator of 21cmfast summary observables*, *Monthly Notices of the Royal Astronomical Society* **527** (2023) 9833.

[64] T.R. Choudhury, A. Paranjape and B. Maity, *A gpr-based emulator for semi-numerical reionization code script: parameter inference from 21 cm data*, *Journal of Cosmology and Astroparticle Physics* **2024** (2024) 027.

[65] Ghara, R., Zaroubi, S., Ciardi, B., Mellema, G., Giri, S. K., Mertens, F. G. et al., *Constraints on the state of the intergalactic medium at $z \sim 8 - 10$ using redshifted 21 cm observations with lofar*, *Astronomy & Astrophysics* **699** (2025) A109.

[66] Y. Mahida, S.K. Yadav, S. Majumdar, L. Noble, C. Shekhar Murmu, S. Dasgupta et al., *From ANN to BNN: Inferring Reionization Parameters using Uncertainty-aware Emulators of 21-cm Summaries*, *arXiv e-prints* (2025) arXiv:2508.13261 [2508.13261].

[67] T. Binnie and J.R. Pritchard, *Bayesian model selection with future 21cm observations of the epoch of reionization*, *Monthly Notices of the Royal Astronomical Society* **487** (2019) 1160.

[68] T. Binnie, X. Zhao, J.R. Pritchard and Y. Mao, *Likelihood-free Model Selection in Cosmic Reionization with Three-dimensional Tomographic 21 cm Lightcone Images*, *arXiv e-prints* (2025) arXiv:2502.08152 [2502.08152].

[69] S. Bharadwaj and S.K. Pandey, *Probing non-gaussian features in the h i distribution at the epoch of re-ionization*, *Monthly Notices of the Royal Astronomical Society* **358** (2005) 968.

[70] G. Mellema, I.T. Iliev, U.-L. Pen and P.R. Shapiro, *Simulating cosmic reionization at large scales – ii. the 21-cm emission features and statistical signals*, *Monthly Notices of the Royal Astronomical Society* **372** (2006) 679.

[71] H. Shimabukuro, S. Yoshiura, K. Takahashi, S. Yokoyama and K. Ichiki, *21 cm line bispectrum as a method to probe cosmic dawn and epoch of reionization*, *Monthly Notices of the Royal Astronomical Society* **458** (2016) 3003.

[72] S. Majumdar, J.R. Pritchard, R. Mondal, C.A. Watkinson, S. Bharadwaj and G. Mellema, *Quantifying the non-gaussianity in the eor 21-cm signal through bispectrum*, *Monthly Notices of the Royal Astronomical Society* **476** (2018) 4007.

[73] R. Mondal, G. Mellema, A.K. Shaw, M. Kamran and S. Majumdar, *The epoch of reionization 21-cm bispectrum: the impact of light-cone effects and detectability*, *Monthly Notices of the Royal Astronomical Society* **508** (2021) 3848.

[74] J. Raste, G. Kulkarni, C.A. Watkinson, L.C. Keating and M.G. Haehnelt, *The 21-cm bispectrum from neutral hydrogen islands at $z \gtrsim 6$* , *Monthly Notices of the Royal Astronomical Society* **529** (2024) 129.

[75] L. Noble, M. Kamran, S. Majumdar, C.S. Murmu, R. Ghara, G. Mellema et al., *Impact of the epoch of reionization sources on the 21-cm bispectrum*, *Journal of Cosmology and Astroparticle Physics* **2024** (2024) 003.

[76] M.M. Friedrich, G. Mellema, M.A. Alvarez, P.R. Shapiro and I.T. Iliev, *Topology and sizes of h ii regions during cosmic reionization*, *Monthly Notices of the Royal Astronomical Society* **413** (2011) 1353.

[77] S.E. Hong, K. Ahn, C. Park, J. Kim, I.T. Iliev and G. Mellema, *2D Genus Topology of 21-cm Differential Brightness Temperature During Cosmic Reionization*, *Journal of Korean Astronomical Society* **47** (2014) 49 [1008.3914].

[78] S. Yoshiura, H. Shimabukuro, K. Takahashi and T. Matsubara, *Studying topological structure of 21-cm line fluctuations with 3d minkowski functionals before reionization*, *Monthly Notices of the Royal Astronomical Society* **465** (2016) 394.

[79] B. Spina, C. Porciani and C. Schimd, *The hi -halo mass relation at redshift $z \sim 1$ from the minkowski functionals of 21-cm intensity maps*, *Monthly Notices of the Royal Astronomical Society* **505** (2021) 3492.

[80] V. Sahni, B.S. Sathyaprakash and S.F. Shandarin, *Shapefinders: A new shape diagnostic for large-scale structure*, *The Astrophysical Journal* **495** (1998) L5.

[81] A. Kapahtia, P. Chingangbam and S. Appleby, *Morphology of 21cm brightness temperature during the epoch of reionization using contour minkowski tensor*, *Journal of Cosmology and Astroparticle Physics* **2019** (2019) 053.

[82] A. Kapahtia, P. Chingangbam, R. Ghara, S. Appleby and T.R. Choudhury, *Prospects of constraining reionization model parameters using minkowski tensors and betti numbers*, *Journal of Cosmology and Astroparticle Physics* **2021** (2021) 026.

[83] K. Kakiichi, S. Majumdar, G. Mellema, B. Ciardi, K.L. Dixon, I.T. Iliev et al., *Recovering the $h\,ii$ region size statistics from 21-cm tomography*, *Monthly Notices of the Royal Astronomical Society* **471** (2017) 1936.

[84] W. Elbers and R.v.d. Weygaert, *Persistent topology of the reionization bubble network – i. formalism and phenomenology*, *Monthly Notices of the Royal Astronomical Society* **486** (2019) 1523.

[85] N. Gillet, A. Mesinger, B. Greig, A. Liu and G. Ucci, *Deep learning from 21-cm tomography of the cosmic dawn and reionization*, *Monthly Notices of the Royal Astronomical Society* **484** (2019) 282
[<https://academic.oup.com/mnras/article-pdf/484/1/282/27509768/stz010.pdf>].

[86] S. Hassan, S. Andrianomena and C. Doughty, *Constraining the astrophysics and cosmology from 21 cm tomography using deep learning with the ska*, *Monthly Notices of the Royal Astronomical Society* **494** (2020) 5761
[<https://academic.oup.com/mnras/article-pdf/494/4/5761/33206590/staa1151.pdf>].

[87] H.J. Hortúa, L. Malagò and R. Volpi, *Constraining the reionization history using bayesian normalizing flows*, *Machine Learning: Science and Technology* **1** (2020) 035014.

[88] D. Prelogović, A. Mesinger, S. Murray, G. Fiameni and N. Gillet, *Machine learning astrophysics from 21 cm lightcones: impact of network architectures and signal contamination*, *Monthly Notices of the Royal Astronomical Society* **509** (2021) 3852
[<https://academic.oup.com/mnras/article-pdf/509/3/3852/41446285/stab3215.pdf>].

[89] X. Zhao, Y. Mao, C. Cheng and B.D. Wandelt, *Simulation-based inference of reionization parameters from 3d tomographic 21 cm light-cone images*, *The Astrophysical Journal* **926** (2022) 151.

[90] S. Neutsch, C. Heneka and M. Brüggen, *Inferring astrophysics and dark matter properties from 21 cm tomography using deep learning*, *Monthly Notices of the Royal Astronomical Society* **511** (2022) 3446
[<https://academic.oup.com/mnras/article-pdf/511/3/3446/42565806/stac218.pdf>].

[91] A. Ore, C. Heneka and T. Plehn, *SKATR: A self-supervised summary transformer for SKA*, *SciPost Phys.* **18** (2025) 155.

[92] B. Schosser, C. Heneka and T. Plehn, *Optimal, fast, and robust inference of reionization-era cosmology with the 21cmPIE-INN*, *SciPost Phys. Core* **8** (2025) 037.

[93] P.R. Posture, Y. Mahida, S. Majumdar and L. Noble, *CosmoUiT: A Vision Transformer-UNet Hybrid for Fast and Accurate Emulation of 21-cm Maps from the Epoch of Reionization*, *arXiv e-prints* (2025) arXiv:2510.01121 [[2510.01121](https://arxiv.org/abs/2510.01121)].

[94] S.F. Shandarin, *Percolation theory and the cell-lattice structure of the universe*, *Pisma v Astronomicheskii Zhurnal* **9** (1983) 195.

[95] A. Klypin and S.F. Shandarin, *Percolation Technique for Galaxy Clustering*, *The Astrophysical Journal* **413** (1993) 48.

[96] S. Dasgupta, S.K. Pal, S. Bag, S. Dutta, S. Majumdar, A. Datta et al., *Interpreting the $h\,ii$ 21-cm cosmology maps through largest cluster statistics. part i. impact of the synthetic ska1-low observations*, *Journal of Cosmology and Astroparticle Physics* **2023** (2023) 014.

[97] E. Regős, V. Springel, S. Bose, B. Hadzhiyska and C. Hernández-Aguayo, *Percolation statistics in the millenniumtng simulations*, *The Astrophysical Journal* **974** (2024) 126.

[98] S.K. Pal, S. Dasgupta, A. Datta, S. Majumdar, S. Bag and P. Sarkar, *Interpreting the hi 21 cm cosmology maps through largest cluster statistics. part ii. impact of the realistic foreground and instrumental noise on synthetic ska1-low observations*, *Journal of Cosmology and Astroparticle Physics* **2025** (2025) 096.

[99] S. Majumdar, H. Jensen, G. Mellema, E. Chapman, F.B. Abdalla, K.-Y. Lee et al., *Effects of the sources of reionization on 21-cm redshift-space distortions*, *Monthly Notices of the Royal Astronomical Society* **456** (2015) 2080.

[100] T.R. Choudhury, M.G. Haehnelt and J. Regan, *Inside-out or outside-in: the topology of reionization in the photon-starved regime suggested by $ly\alpha$ forest data*, *Monthly Notices of the Royal Astronomical Society* **394** (2009) 960.

[101] K.K. Datta, G. Mellema, Y. Mao, I.T. Iliev, P.R. Shapiro and K. Ahn, *Light-cone effect on the reionization 21-cm power spectrum*, *Monthly Notices of the Royal Astronomical Society* **424** (2012) 1877.

[102] K.K. Datta, H. Jensen, S. Majumdar, G. Mellema, I.T. Iliev, Y. Mao et al., *Light cone effect on the reionization 21-cm signal – ii. evolution, anisotropies and observational implications*, *Monthly Notices of the Royal Astronomical Society* **442** (2014) 1491.

[103] P. La Plante, N. Battaglia, A. Natarajan, J.B. Peterson, H. Trac, R. Cen et al., *Reionization on large scales. iv. predictions for the 21 cm signal incorporating the light cone effect*, *The Astrophysical Journal* **789** (2014) 31.

[104] K. Zawada, B. Semelin, P. Vonlanthen, S. Baek and Y. Revaz, *Light-cone anisotropy in the 21 cm signal from the epoch of reionization*, *Monthly Notices of the Royal Astronomical Society* **439** (2014) 1615.

[105] R. Ghara, K.K. Datta and T.R. Choudhury, *21 cm signal from cosmic dawn – ii. imprints of the light-cone effects*, *Monthly Notices of the Royal Astronomical Society* **453** (2015) 3143.

[106] R. Mondal, S. Bharadwaj and K.K. Datta, *Towards simulating and quantifying the light-cone eor 21-cm signal*, *Monthly Notices of the Royal Astronomical Society* **474** (2017) 1390.

[107] C.S. Murmu, S. Majumdar and K.K. Datta, *Cii and hi 21-cm line intensity mapping from the eor: impact of the light-cone effect on auto and cross-power spectra*, *Monthly Notices of the Royal Astronomical Society* **507** (2021) 2500.

[108] I.T. Iliev, G. Mellema, K. Ahn, P.R. Shapiro, Y. Mao and U.-L. Pen, *Simulating cosmic reionization: how large a volume is large enough?*, *Monthly Notices of the Royal Astronomical Society* **439** (2014) 725.

[109] M. Ricotti, *Did globular clusters reionize the universe?*, *Monthly Notices of the Royal Astronomical Society* **336** (2002) L33.

[110] R.M. Thomas, S. Zaroubi, B. Ciardi, A.H. Pawlik, P. Labropoulos, V. Jelić et al., *Fast large-scale reionization simulations*, *Monthly Notices of the Royal Astronomical Society* **393** (2009) 32.

[111] N.Y. Gnedin, *Cosmic reionization on computers. i. design and calibration of simulations*, *The Astrophysical Journal* **793** (2014) 29.

[112] R. Ghara, T.R. Choudhury and K.K. Datta, *21 cm signal from cosmic dawn: imprints of spin temperature fluctuations and peculiar velocities*, *Monthly Notices of the Royal Astronomical Society* **447** (2015) 1806.

[113] S. Majumdar, G. Mellema, K.K. Datta, H. Jensen, T.R. Choudhury, S. Bharadwaj et al., *On the use of seminumerical simulations in predicting the 21-cm signal from the epoch of reionization*, *Monthly Notices of the Royal Astronomical Society* **443** (2014) 2843.

- [114] J. Harnois-Déraps, U.-L. Pen, I.T. Iliev, H. Merz, J.D. Emberson and V. Desjacques, *High-performance p3m n-body code: cubep3m*, *Monthly Notices of the Royal Astronomical Society* **436** (2013) 540.
- [115] M. McQuinn, *Constraints on x-ray emissions from the reionization era*, *Monthly Notices of the Royal Astronomical Society* **426** (2012) 1349.
- [116] W.L.W. Sargent, C.C. Steidel and A. Boksenberg, *A Survey of Lyman-Limit Absorption in the Spectra of 59 High-Redshift QSOs*, *The Astrophysical Journal Supplement* **69** (1989) 703.
- [117] K.M. Lanzetta, *Evolution of High-Redshift Lyman-Limit Absorption Systems*, *The Astrophysical Journal* **375** (1991) 1.
- [118] J.V. Sheth, V. Sahni, S.F. Shandarin and B.S. Sathyaprakash, *Measuring the geometry and topology of large-scale structure using surfgen: methodology and preliminary results*, *Monthly Notices of the Royal Astronomical Society* **343** (2003) 22.
- [119] E. Chernyaev, *Marching cubes 33: construction of topologically correct isosurfaces*, Tech. Rep. CERN-CN-95-17, CERN, Geneva (1995).